X-615-69-134

PREPRINT

NASA TM X- 63553

THE ION-WAKE EXPERIMENT ON GEMINI 10

APRIL 1969

GODDARD SPACE FLIGHT CENTER
GREENBELT, MARYLAND

X-615-69-134

THE ION-WAKE EXPERIMENT ON GEMINI 10

Ballard E. Troy, Jr.
Ionospheric and Radio Physics Branch
Laboratory for Space Sciences

April 1969

GODDARD SPACE FLIGHT CENTER
Greenbelt, Maryland

CONTENTS

ILLUSTRATIONS

TABLES

THE ION-WAKE EXPERIMENT ON GEMINI 10

INTRODUCTION

The interaction between an orbiting satellite and its surrounding medium[1-21] has been widely investigated. An understanding of this interaction is important to proper interpretation of information from the satellite's direct-measurement experiments. One aspect of this interaction—the wake, or ion-depleted region behind the spacecraft—results from a discrepancy between satellite velocity and the thermal velocity of charged particles in the surrounding ionosphere. In low orbits, satellite velocity is roughly an order-of-magnitude greater than positive-ion thermal velocity and an order-of-magnitude less than electron thermal velocity. Rapid satellite motion through the charged particles sweeps the ions out of the wake, and, when the Debye length is short compared to the satellite dimensions, decreases electron density in the wake although the electrons move too fast to be entirely swept out.

Theoretical studies to predict properties of the wake[1-7] often simplify or ignore some of the problems involved (such as magnetic fields or photoemissions). Most of the experiments on wakes simulated the ionosphere in the laboratory and scaled experiment parameters.[8-10] Satellite experiments were usually mounted flush with the satellite skin[11,12,21] and have produced wake data. Exceptions were the experiments on the Ariel satellite[13,14,15] and the electron probes of Brace[17] and Oya.[20] Until 1966, however, no experiments gathered wake data at varying distances from a satellite; no satellite observed independently the wake of another.

The Gemini-Agena rendezvous flights offered the first opportunity for performing a wake experiment with two independent vehicles. Early in 1965, the author proposed a wake experiment using the Gemini-Agena two-body system, in which instruments mounted on the Agena vehicle would observe the ionospheric wake of the Gemini spacecraft. Previous commitments to existing NASA projects and the imminent conclusion of the Gemini program prevented the allocation of GSFC facilities or manpower to the proposed experiment. The Manned Spacecraft Center, however, contracted the experiment to Electro-Optical Systems, Inc. Dr. David Medved, principal investigator, and Ballard E. Troy, Jr., co-investigator, had access to the data and participated in the data analysis.

EXPERIMENT OBJECTIVE AND DESCRIPTION

The Gemini ion-wake experiment (denoted S-26 among Gemini experiments) was designed to observe, with instruments mounted on the Agena target vehicle,

the ionospheric charged particles in the wake region of the Gemini spacecraft and, by special maneuvers, to determine the extent of the wake.

Figure 1 is a schematic drawing of the instruments used, multiple-grid planar ion and electron collectors. Six circular wire-mesh grids and a circular collector plate were mounted in a rectangular chassis in each sensor.

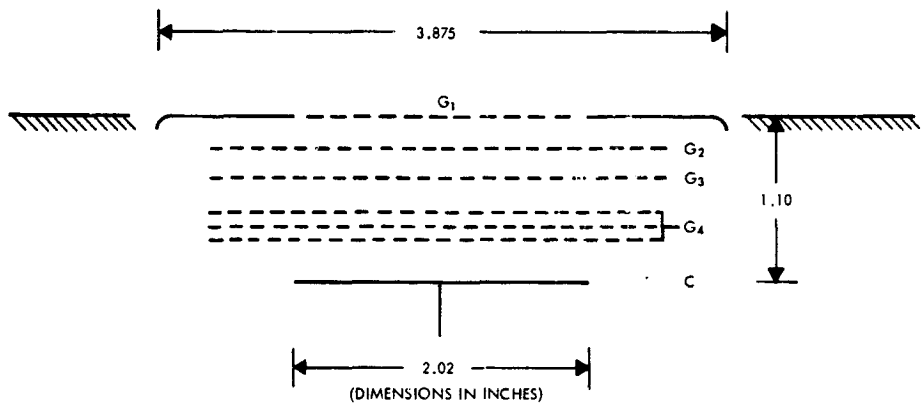

Figure 1. S-26 Ion and Electron Sensors, Schematic Drawing

The outer grid was smaller than the others; it was mounted flush with a circular guard ring which was physically separate from the chassis skin. Appropriate voltages were impressed on the grids to collect the desired type of charged particle, either electron or positive ion; to exclude particles of opposite charge; and to suppress emission of photoelectrons from the collector. Figures 2 and 3 illustrate the voltages.

Grid 3 had a 3840-Hz square-wave chopping voltage, causing the collector to see an ac current of the same frequency. An ac electrometer amplified this ac current but did not amplify dc current signals, such as photoemission from the inner grids. Grids 4, 5, and 6—tied to the same potential—provided capacitive separation of the collector from the ac signal on grid 3.

The voltage on the outer grid of the electron sensor was swept, in 0.2-volt steps, in 1 second, from -3.0 volts to +8.8 volts. This sweep modulated the electron current and made possible the determination of electron-energy distribution, electron density, and vehicle electrical potential. The ion current, however, was not modulated and only ion density (not energy distribution) could be determined.

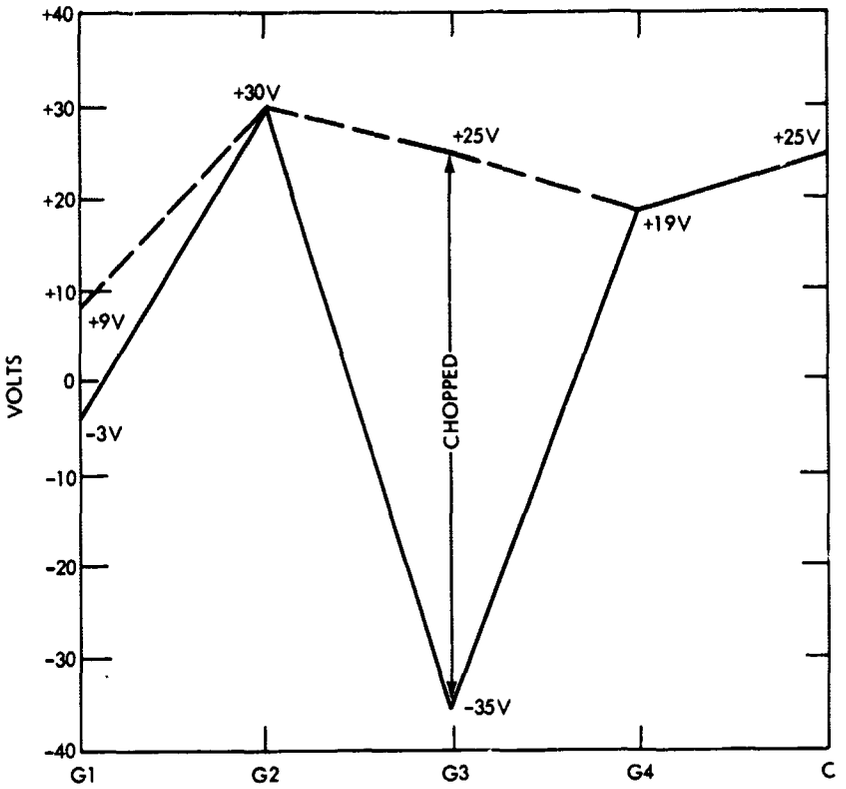

NOTES:
Chopping frequency on grid 3 is 3840 Hz square wave.
G1 is stepped from +9 to -3 volts in 60 equal steps and set at -12 volts during calibration and sync.
G4 is a triple grid to completely isolate G3 from collector.

Figure 2. Electron-Sensor Grid Potentials

The collected currents were sent to the Agena telemetry systems for direct transmission to ground or to the Agena tape recorder for later transmission. All data could not be collected because there were too few ground stations and tape recorder capacity was only 20 minutes. The value of the retarding voltage on the outer grid was not telemetered; it was inferred from the shape of the electron curve. Four calibration points allowed identification of the beginning of each curve. Data were available to the experimenters in tabulated form or on magnetic tape. Because an extremely large amount of information was taken in this flight, not all data received were decommutated.

After being reduced, the data were correlated with the relative position of the Agena to the Gemini, which proved to be the most difficult part of the data-analysis problem. No system was available for uniquely determining at all times the relative Agena-Gemini position. The primary instrument, a movie camera, looked out one

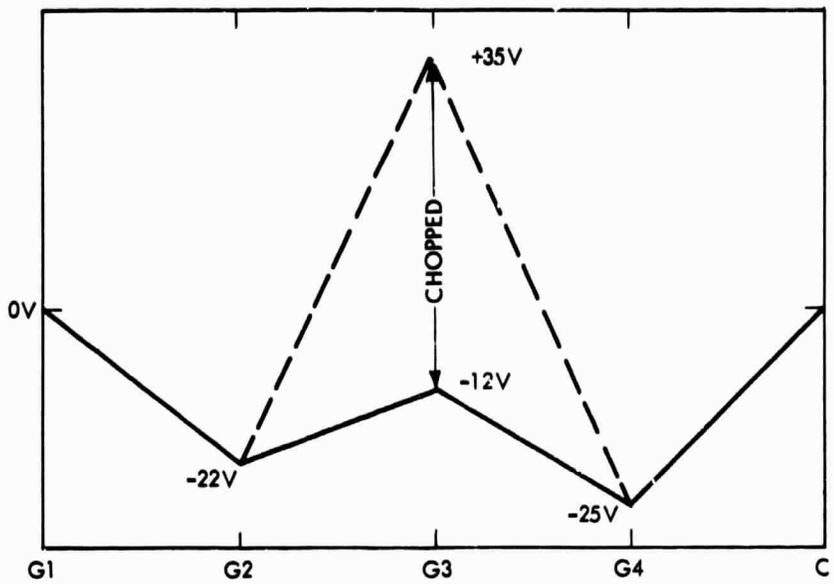

NOTES:
Chopping frequency on grid 3 is 3840-Hz square wave.
G1 goes to +35 volts during calibration.
G4 is a triple grid to completely isolate G3 from the collector.

Figure 3. Ion-Sensor Grid Potentials

Gemini window along the spacecraft axis and operated when the Agena was in view. The on-board thruster firing record, voice tape of the astronauts, spacecraft-attitude information, and on-board radar record were also used in this correlation.

Figure 4 shows the locations of the two ion sensors and one electron sensor mounted on the target docking adapter (TDA) of the Agena. One ion sensor (in-board) with its grid normal or look direction parallel to the Agena axis was placed inside the TDA looking out the docking cone. The electron sensor and other ion sensor (outboard), mounted flush with the edge of the Agena's skin, looked perpendicularly to the axis.

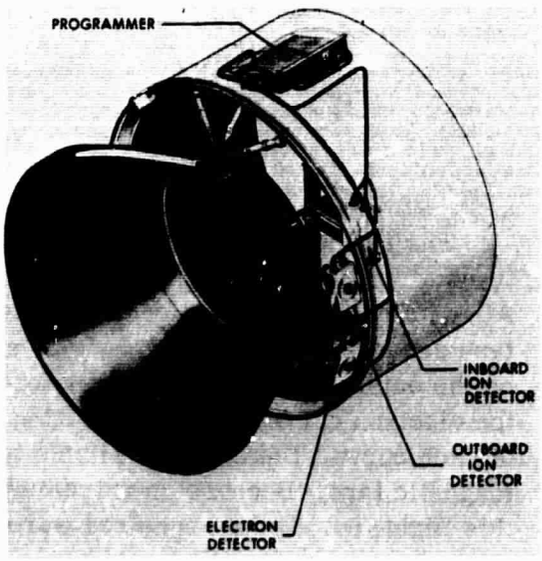

Figure 4. Sensor Locations on Agena TDA

When in orbit and undocked, the attitude-control system of the Agena allowed only four stable positions (Figure 5). The Agena axis was always parallel to the earth's surface and either parallel or normal to the velocity vector. Because the ion sensors had to look close to the velocity vector for accurate density determination, the positions of TDA forward and TDA south were the only ones which allowed proper simultaneous operation of the electron sensor and one ion sensor.

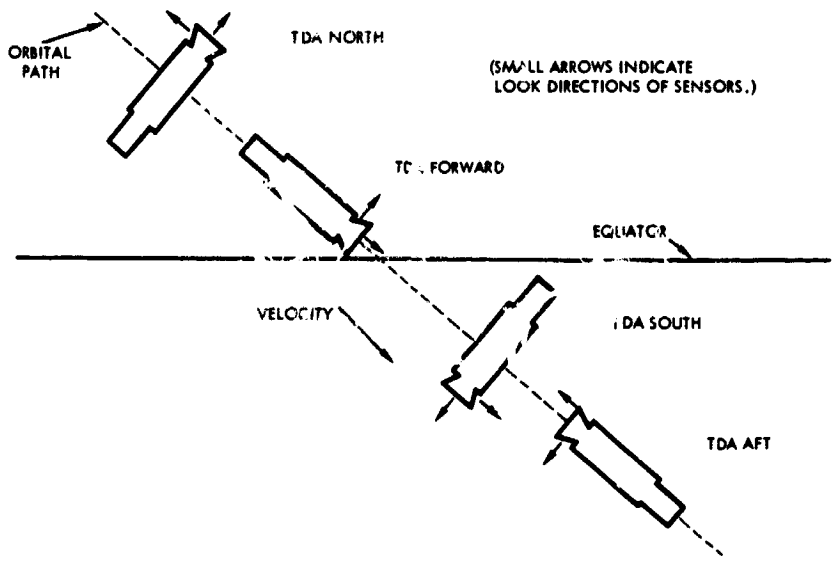

Figure 5. Undocked Agena Orientations Permissible in Orbit

A series of preplanned maneuvers to map the wake laterally and longitudinally were scheduled for the flight. In these maneuvers, the Agena would be either TDA forward or TDA south and behind the Gemini, which was to perform the special maneuvers. Figure 6 shows their planned relative positions.

The diameter of the Agena was 5 feet; that of the Gemini was 10 feet at its widest part. Whenever the Agena was TDA forward and coaxial with the Gemini (as in Figure 6a), the electron sensor and outboard ion sensor were 2.5 feet inside the geometrical shadow wake of the Gemini.

Analysis Method

The analysis method used is standard for planar probes. Figure 7 is a representative S-26 electron plot.

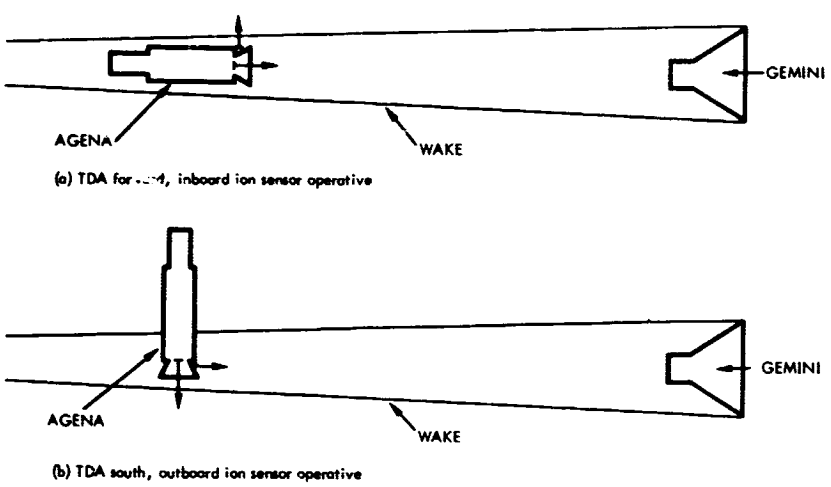

Figure 6. Primary Configurations for Wake Investigation

In the retarding region, the current generated by the thermal electrons is assumed to have the following form:

$$I = I_0 e^{e\phi/kT_e} \qquad \phi < 0 \tag{1}$$

where

$\phi = \phi_s + \phi_g$ = grid-ionosphere potential

ϕ_s = satellite-ionosphere potential

ϕ_g = grid-satellite potential (retarding potential)

T_e = electron temperature

I_0 = current at the break point ($\phi = 0$)

By subtracting the background, the total current may be resolved into the thermal component and the suprathermal (background) component. The slope of the thermal component determines T_e:

$$T_e = \left(\frac{k}{e}\frac{d\,\ell n\, I}{d\phi_g}\right)^{-1} \tag{2}$$

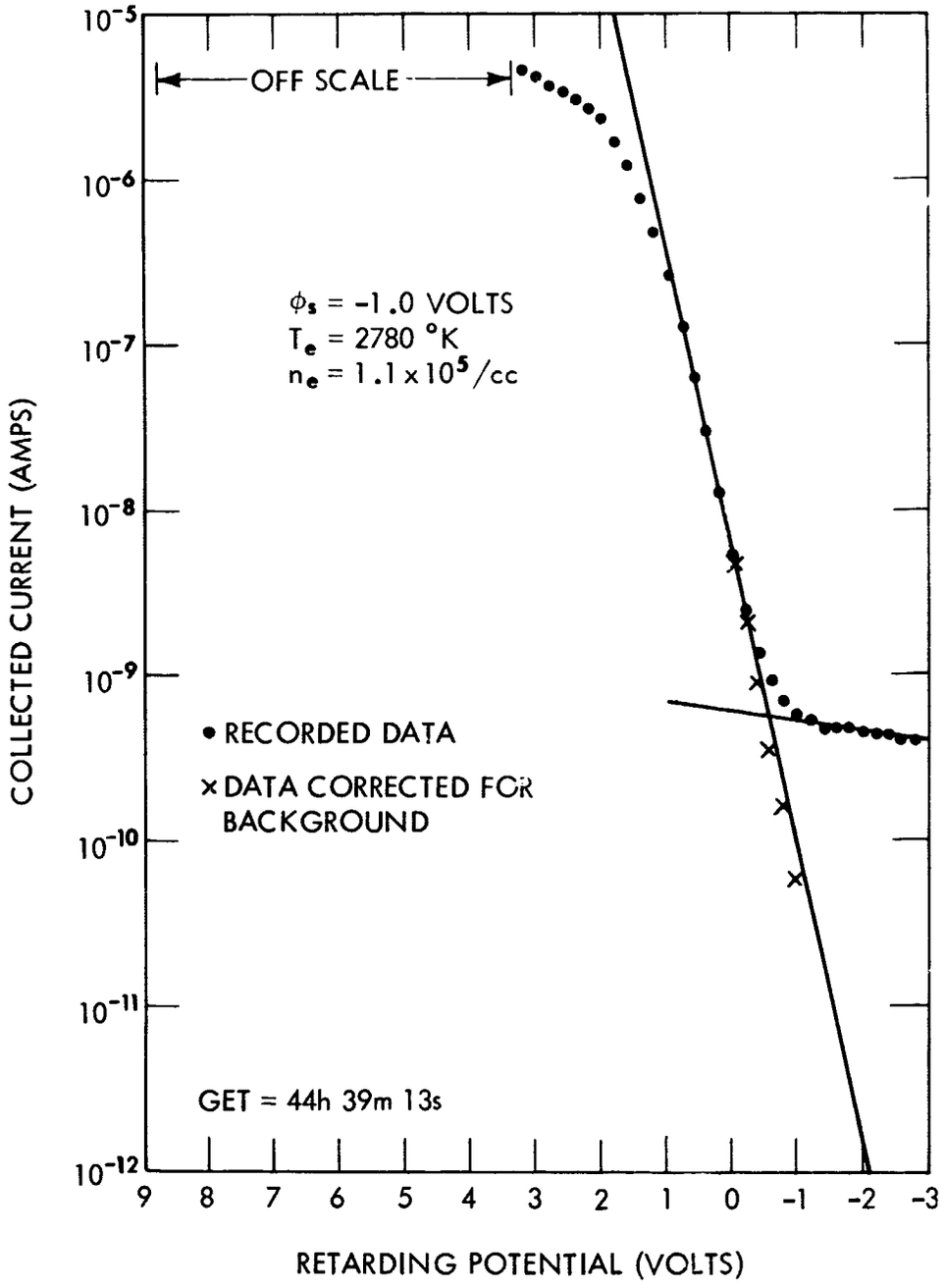

Figure 7. Representative Electron Plot from S-26

The I curve breaks away from an exponential form at $\phi = 0$, determining the satellite potential as $\phi_s = -\phi_g$. At the break point, $I = I_0$, from which the electron density n_e can be determined:

$$n_e = \frac{2\sqrt{\pi}\, I_0}{A e \alpha_e a_e} \tag{3}$$

where

A = collection area

α_e = total electron transparency

$a_e = \sqrt{2kT_e/m_e}$ = most probable electron velocity

Because uncertainty exists in determining the exact break point, about a ± 25-percent uncertainty exists in determining n_e.

The ion density n_+ is determined from the ion current I_+. For the ion sensor looking directly forward along the velocity vector,

$$n_+ = \frac{I_+}{A\alpha_+ eV_s}$$

where

α_+ = total positive ion transparency

V_s = satellite velocity

For the ion sensor looking perpendicular to the velocity vector,

$$n_+ = \frac{2\sqrt{\pi}\, I_+}{Ae\, \alpha_+\, a_+}$$

where

$a_+ = \sqrt{2kT_+/m_+}$ = most probable ion velocity

Because, ion temperature T_+ is not determined experimentally, it is assumed that $T_+ = T_e$.

Calculation of Effective Collection Area for Electrons

If the sensor aperture and collector are equal in size, some particles (particularly electrons, with their isotropic velocity distribution relative to the satellite) will pass through all grids without hitting the collector. Calculations were made in two limiting cases to determine the effective collection area for electrons. In the one case, the electrons were assumed to travel through the sensor, undeviated by the internal electric fields. In the other case, the electrons within the sensor were assumed to have a velocity normal to the collector, the velocity determined by accelerating voltages on the grids; the electron's characteristic thermal velocity was parallel to the collector. The effective collection areas for the two cases were $0.35\,A_0$ and $0.86\,A_0$, respectively, where A_0 was the aperture area ($0.35A_0$ was used to determine n_e, because it agreed well with electron densities determined from ionosondes and minimized the difference between n_+ and n_e).

PERFORMANCE

Agena 10 was launched July 18, 1966, at 2040 UT and the Gemini craft at 2220 UT, into orbits with inclinations of about 29 degrees. After orbital changes, the two vehicles rendezvoused and docked at about 0540 SGET (spacecraft ground elapsed time, measured from the launch of the Gemini). Because the Gemini had consumed an excessive amount of fuel, the planned S-26 maneuvers were cancelled to conserve the remaining fuel.

The two craft remained docked until 4440 SGET (1900 UT on July 20) when they undocked at a 385-km altitude with the Agena oriented TDA forward. By firing its onboard thrusters, the Gemini moved away from the Agena in the velocity direction, causing the Agena to move linearly backward through the length of the Gemini wake (Figure 6a). This was the only maneuver on the flight when substantial wake data were taken. The rest of this report analyzes these wake data and other data which clarify the wake information.

RESULTS

Comparison with Ground-Based Data

To compare directly n_e determined by S-26 and n_e determined by other methods, ionosonde data were sought from ground-based stations and the topside-sounder satellites (Alouette I and Alouette II). S-26 and Alouette could not make a simultaneous determination of n_e at the same location. However, several comparisons of n_e from S-26 and from ionograms were available; Table 1 lists the results.

Table 1.
Comparison of n_e From S-26 and From Ionograms

IONOGRAM								S-26						
DATE	UT	SGET	LST	STA	LAT	LONG	ALT	n_e^1	IDA ATT	SGET	LAT	LONG	ALT (KM)	n_e^4
(July) 18	2218	140A*	1718	CK	28°	-80°	F2	6.6	YAW	140A*	28°	-80°	298	9.0
18	2218	140A*	1718	GB	26°	-78°	F2	6.4	YAW	140A*	28°	-78°	298	5.8
18	2330	110	1330	HAW	20°	-156°	299 km	6.4	South	116	22°	-156°	299	8.0
18	2345	125	1645	WS	32°	-106°	261	4.3	South	130	29°	-106°	298	4.5
18	2400	134	1900	JA	18°	-76°	255	9.7	South	135	22°	-76°	295	5.8
20	2115	4655	1115	HAW	20°	-156	343	6.9	FWD	4730	18°	-156°	385	6.6
20	2215	4755	1213	HAW	20°	-156	349	8.9	FWD	4730	18°	-156°	385	6.6
20	2245	4825	1545	WS	32°	-106°	258	5.4	FWD	4743	29°	-106°	392	3.5

*Agena time
**n_e given in 10^5/cc

CK-Cape Kennedy; GB-Grand Bahama; HAW-HAWAII; WS-White Sands; JA-Jamaica

On several of the occasions listed in Table 1, the maximum height of n_e as determined by the ionogram was below the Agena altitude. Because ionosonde data cannot determine n_e above the F2 maximum, the Agena was possibly above F2 maximum during these periods. Where direct comparisons were made, n_e (S-26) was roughly 20 percent greater than n_e (ionosonde). The Agena was undocked for all times listed in Table 1.

Observations of the Ambient Ionosphere

Data taken by all three sensors were compared for periods during which the undisturbed ionosphere could be observed (early in the mission before docking and later in the mission after undocking). Comparisons were made for both TDA forward and TDA south.

Figures 8 through 11 are plots of currents from the sensors during TDA-forward periods versus local time, for portions of one orbit before docking and three orbits after undocking. The electron current used was I_0, the current at the break in the electron curve. Figure 8 shows that the currents were all roughly proportional before 1100 local time, after which I_+ (inboard) dropped while the outboard currents increased. This divergence between I_+ (inboard) and the other outboard sensor currents was also present after undocking (Figures 9-11).

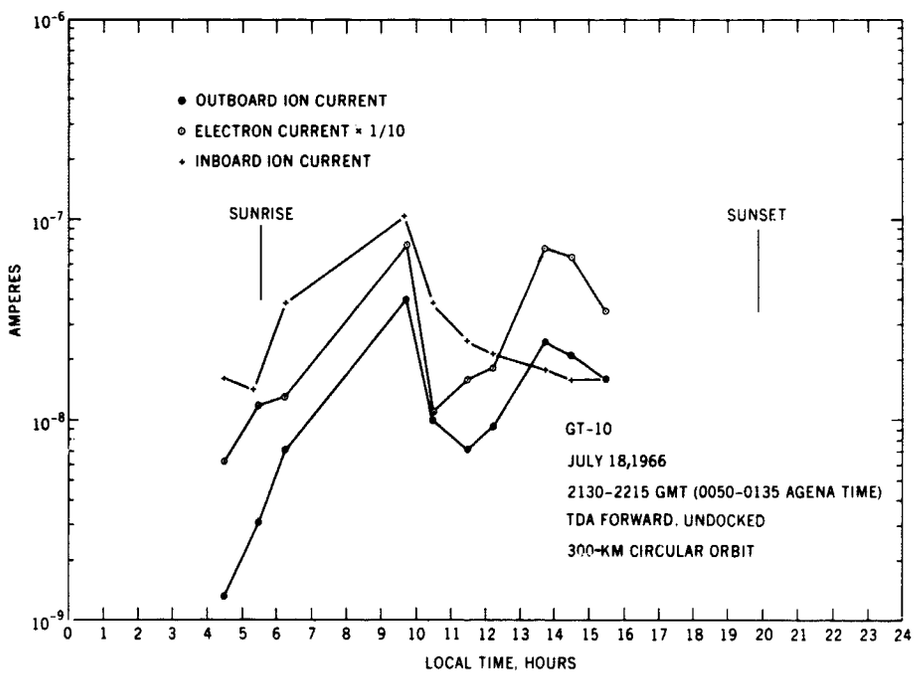

Figure 8. Sensor Currents, 0050-0135 Agena Time

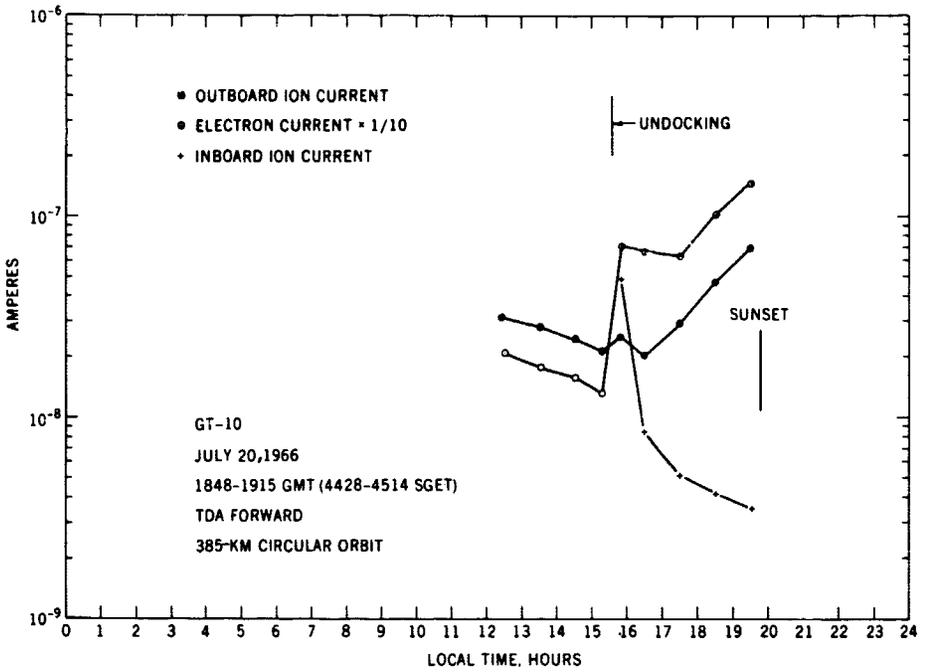

Figure 9. Sensor Currents, 4428-4514 SGET

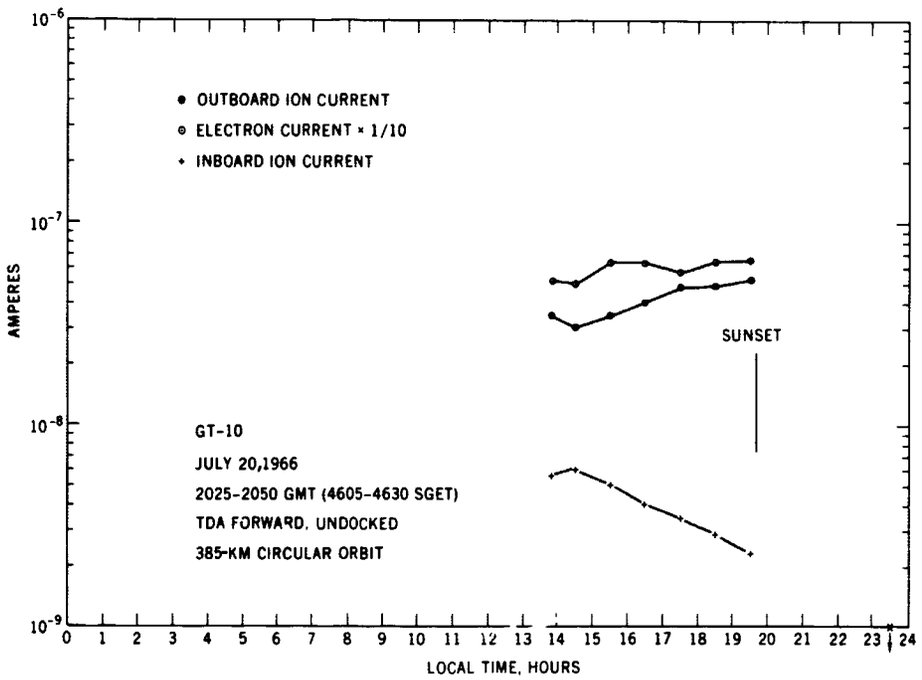

Figure 10. Sensor Currents, 4605-4630 SGET

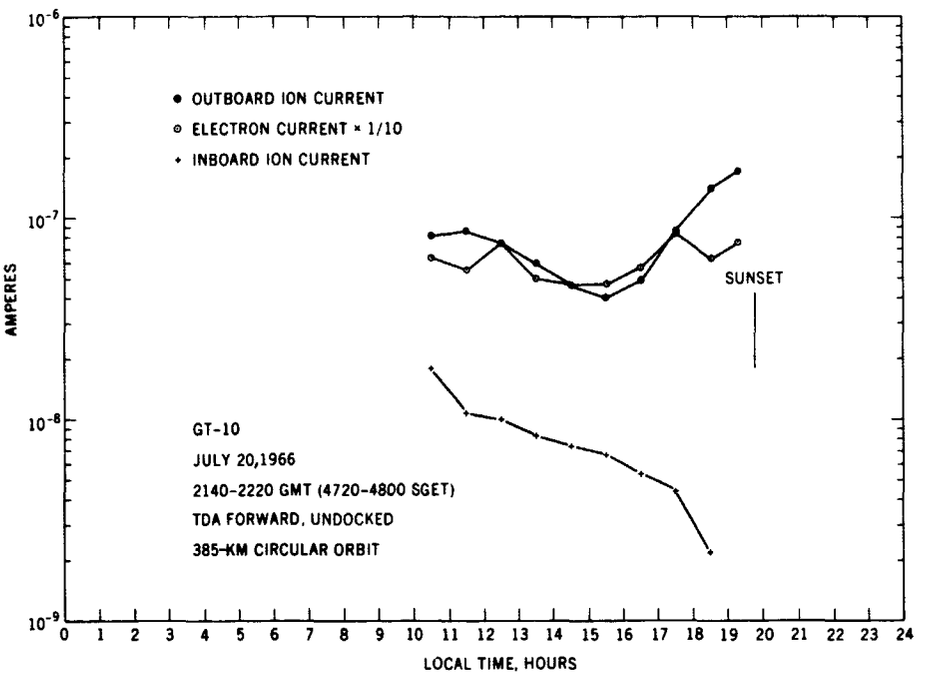

Figure 11. Sensor Currents, 4720-4800 SGET

Figure 12 shows n_e and n_+ (inboard) for the time period covered in Figure 8. The two densities were roughly equal before 1100 local time, but n_+ (inboard) density became much less than n_e afterwards. This discrepancy in densities continued later in the flight (time periods of Figures 9-11), except perhaps immediately after undocking. For the same period, n_+ (outboard), determined by equation 5 (not plotted), was generally proportional to n_e but greater than n_e by a factor of 2-4.

For two TDA south periods, n_e and n_+ (outboard) were derived (Figures 12-13). Before docking and after undocking, n_+ (outboard) was greater than n_e by a factor of 2.

Correlations between the S-26 ambient densities and other parameters have been noted. When densities of Figure 12 and the following orbit (not shown) are plotted versus a latitude scale, their temporal variations are observations of the geomagnetic anomaly. Also, a general inverse relationship exists between n_e and T_e throughout the ambient data analyzed.

These comparisons reveal the following experiment performance information:

- Electron density determined by S-26 is equal to that determined by ionosondes, within experimental error.

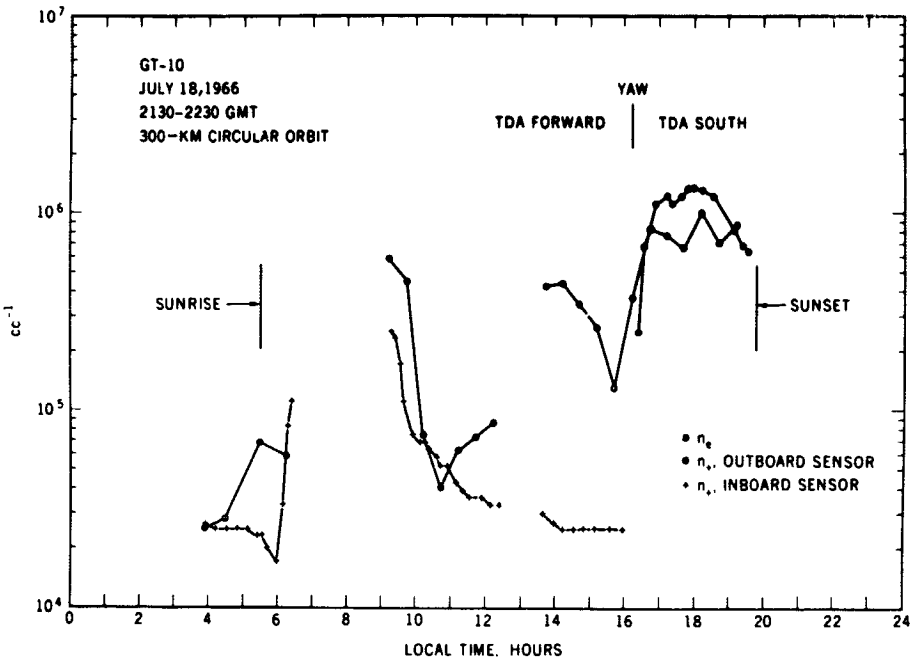

Figure 12. Ion and Electron Densities, 0050-0150 Agena Time

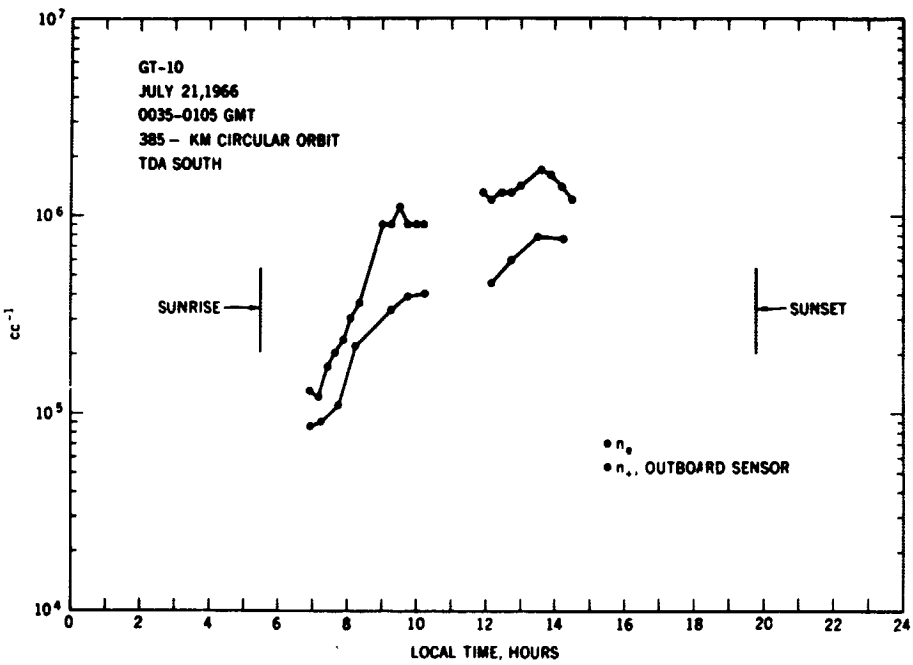

Figure 13. Ion and Electron Densities, 5015-5045 SGET

- n_+ (inboard) agrees reasonably with n_e only during the first Agena orbits and immediately after undocking; it is much too low at other times.

- n_+ (outboard) is proportional to n_e for both TDA south and TDA forward, but is greater than n_e by a factor of 2-4.

- Added confidence in the correctness of n_e can be gained by its change with other parameters, namely latitude (geomagnetic anomaly) and T_e (inverse relation).

Observation of the Wake During Undocking

Undocking occurred at 44h 40m 15.8s SGET, with the Gemini firing its thrusters and moving away from the Agena along the velocity vector. Figure 14 illustrates the ion-sensor currents collected during the undocking, with thruster firings shown. The thruster exhaust apparently caused an immediate drop in the ion currents, which recovered within about 1 second after the firing stopped.

Data derived from electron and inboard ion sensors in the periods free of firing effects were used to compute the parameters n_e, T_e, n_+ (inboard), and ϕ_s

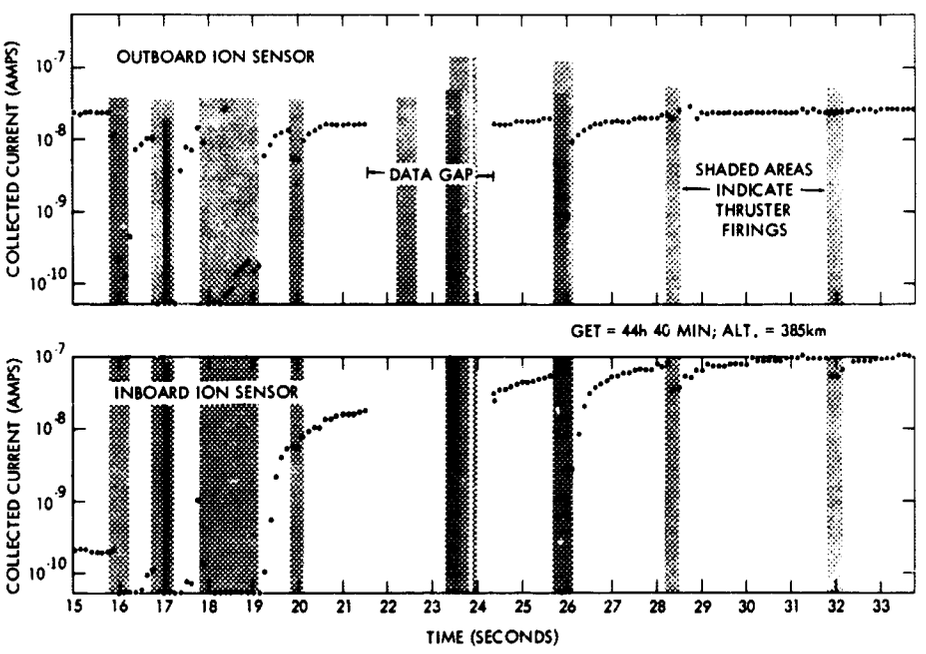

Figure 14. Ion-Sensor Currents During Undocking

(Figure 15). Each parameter changed smoothly after undocking, and each parameter except n_+ (inboard) achieved a stable value before 44h 41m SGET, when the Agena was apparently free of the Gemini's wake.

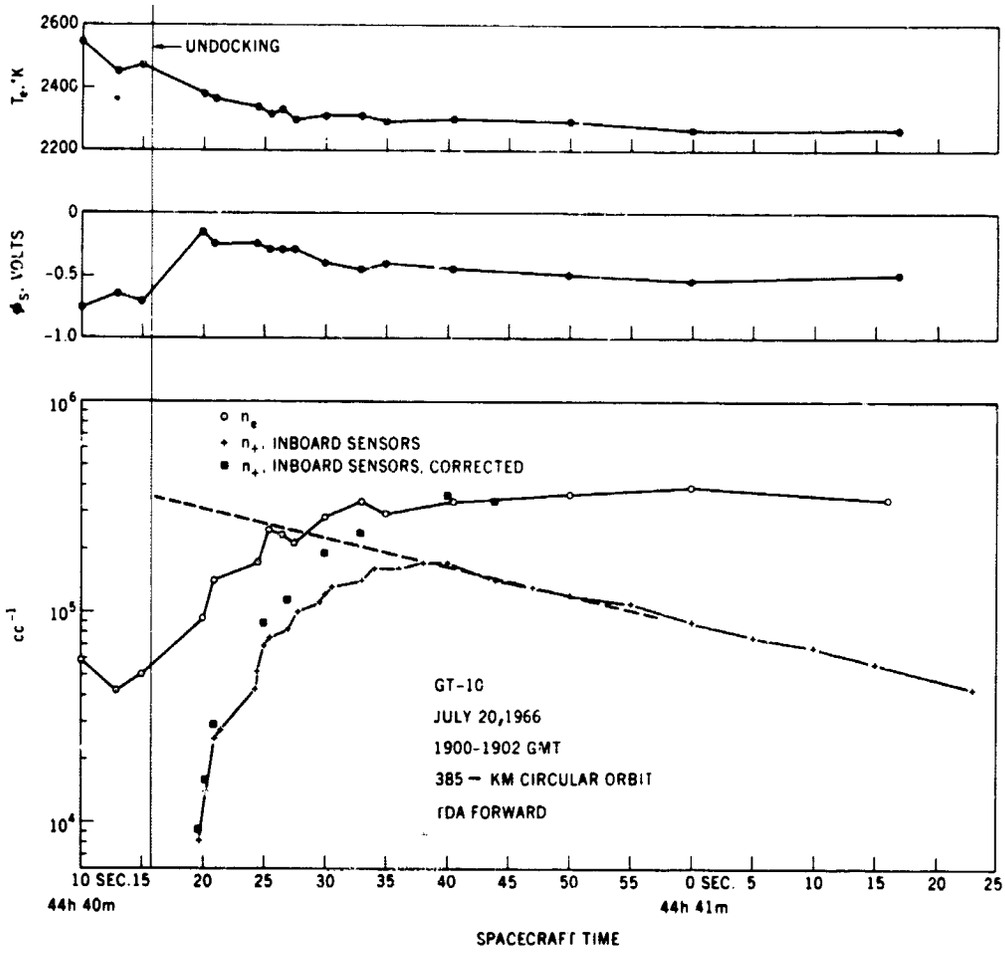

Figure 15. ϕ_s, T_e, n_+, and N_e During Undocking

The densities initially increased as the Agena drew away but, after 44h 10m 40s SGET, n_+ (inboard) began an exponential decrease, with a time constant of 32 seconds. This decrease was slow compared to the previous increase, and occurred when n_e had reached a constant value. Extrapolating the decrease backward to the moment of undocking gives a value of n_+ (inboard) equal to the stable value achieved by n_e; this value indicates that the variation of n_+ (inboard) after undocking is the product of the emergence from the wake, causing an increase, and another effect, causing a decrease.

The form of the decreasing effect is known, and can be used to correct the n_+ (inboard) measurements for the effect. The form is

$$n_+(t) = n_+(t_0)e^{-(t-t_0/32)}$$

Multiplying the values of n_+ (inboard) by $e^{t-t_0/32}$ (where t_0 is the undocking time and t is the measurement time) produces a corrected ion-density curve (Figure 15). The corrected curve rises monotonically after undocking and levels out at the same value as n_e.

The spacecraft potential showed a net positive change from its value before undocking. T_e decreased in the same period, implying a higher T_e in the wake than outside.

Changes in the Ambient Ionosphere During Undocking

To separate wake effects from possible changes in the ambient ionosphere, T_e and n_e versus local time were plotted for portions of the undocking orbit and the two following orbits (Figures 16 and 17). The curves, which are similar for

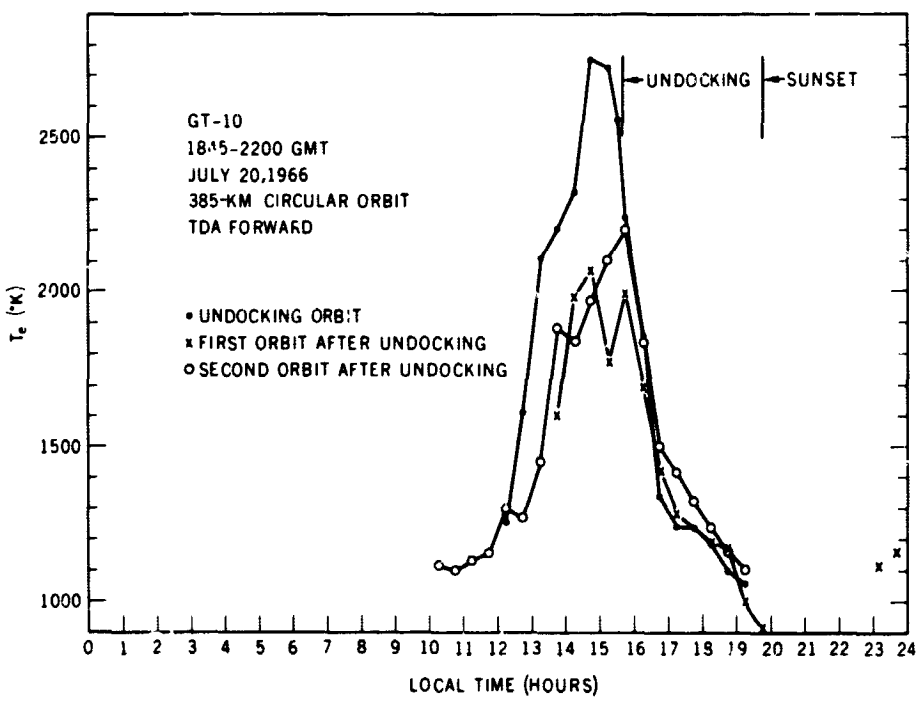

Figure 16. T_e for Undocking Orbit and Two Orbits Following

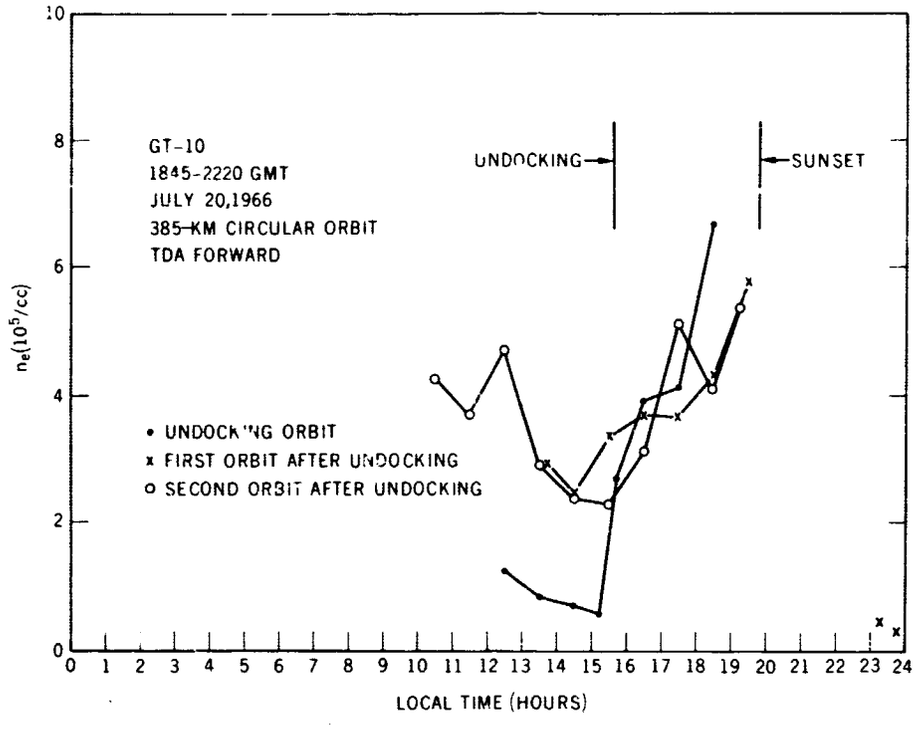

Figure 17. n_e for Undocking Orbit and Two Orbits Following

the three orbits, indicate that the undocking occurred when the ambient n_e was increasing and the ambient T_e decreasing. The ambient change was slow compared to that observed during undocking. T_e was higher and n_e lower for the docked configuration than for the undocked configuration at the same local time.

The geophysical cause of the ambient variation is evident when these data are compared with the Agena latitude variation. On each orbit, the Agena reached its maximum latitude of 29 degrees near 1500 local time, corresponding to the maximum of T_e and the minimum of n_e. The corresponding geomagnetic latitudes showed a maximum of 38 degrees to 40 degrees at the same time. Figure 18 shows T_e versus geomagnetic latitude for the second orbit after undocking. T_e increased with geomagnetic latitude as expected, although the variation was stronger than expected.

Axial Wake Profile

A time-history of the gross Gemini-Agena separation (= 0 at undocking) was derived from the thruster firing history and the known mass of the Gemini. Figure 19 shows T_e, n_e, ϕ_s, and the corrected n_+ (inboard) as functions of this axial separation. In the docked position, the outboard sensors were 18 feet

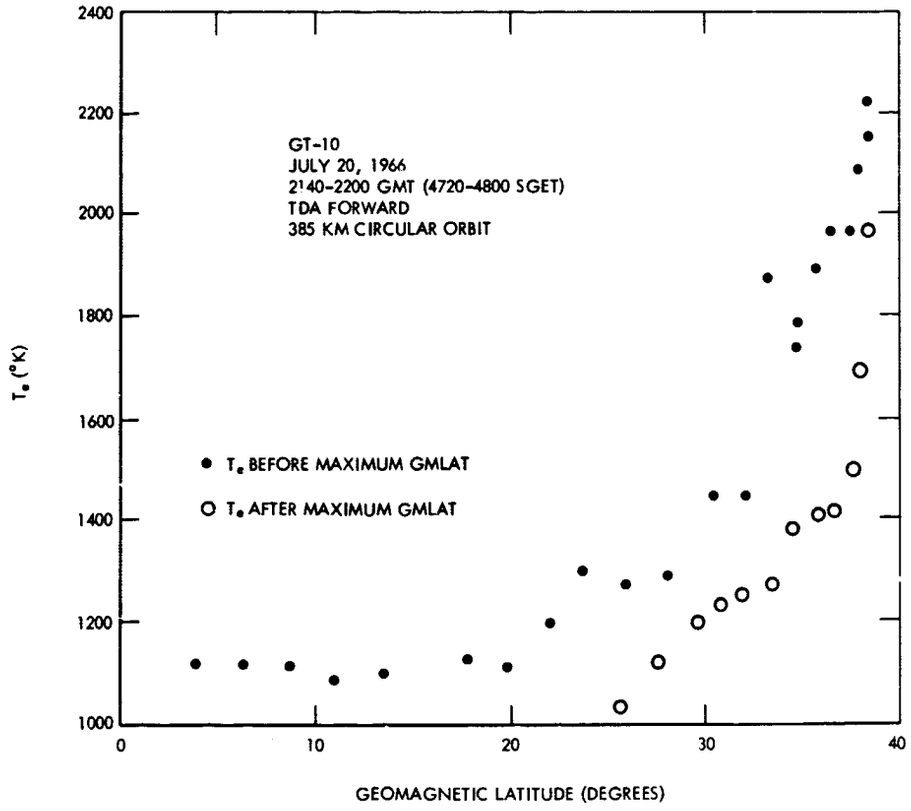

Figure 18. T_e vs. Geomagnetic Latitude for Second Orbit After Undocking

behind the forwardmost portion of the Gemini, where the radius is 5 feet, the largest radius of the Gemini. By using 5 feet as a "characteristic length" R_0, a scale of distance behind the forwardmost position in terms of R_0 was obtained. All parameters reach a constant value on this scale at about $10\,R_0$.

No theoretical calculations of density have been made for the wake of the irregularly shaped Gemini. The S-26 densities may be compared with n_+ from a current theory for a regularly shaped body. Shea[6] has calculated the ratio $N_+ = n_+$ (wake)/n_+ (ambient) for a sphere, assuming a slightly higher ratio of satellite velocity to thermal, ion velocity than that occurring during the Gemini flights. By multiplying N_+ times the ambient density of $3.7 \times 10^5/cm^3$ seen after undocking, a theoretical curve of n_+ (wake) for a 5-foot radius sphere was obtained and plotted in Figure 19. These theoretical densities lie between the corrected n_+ (inboard) and n_e, as would be expected.

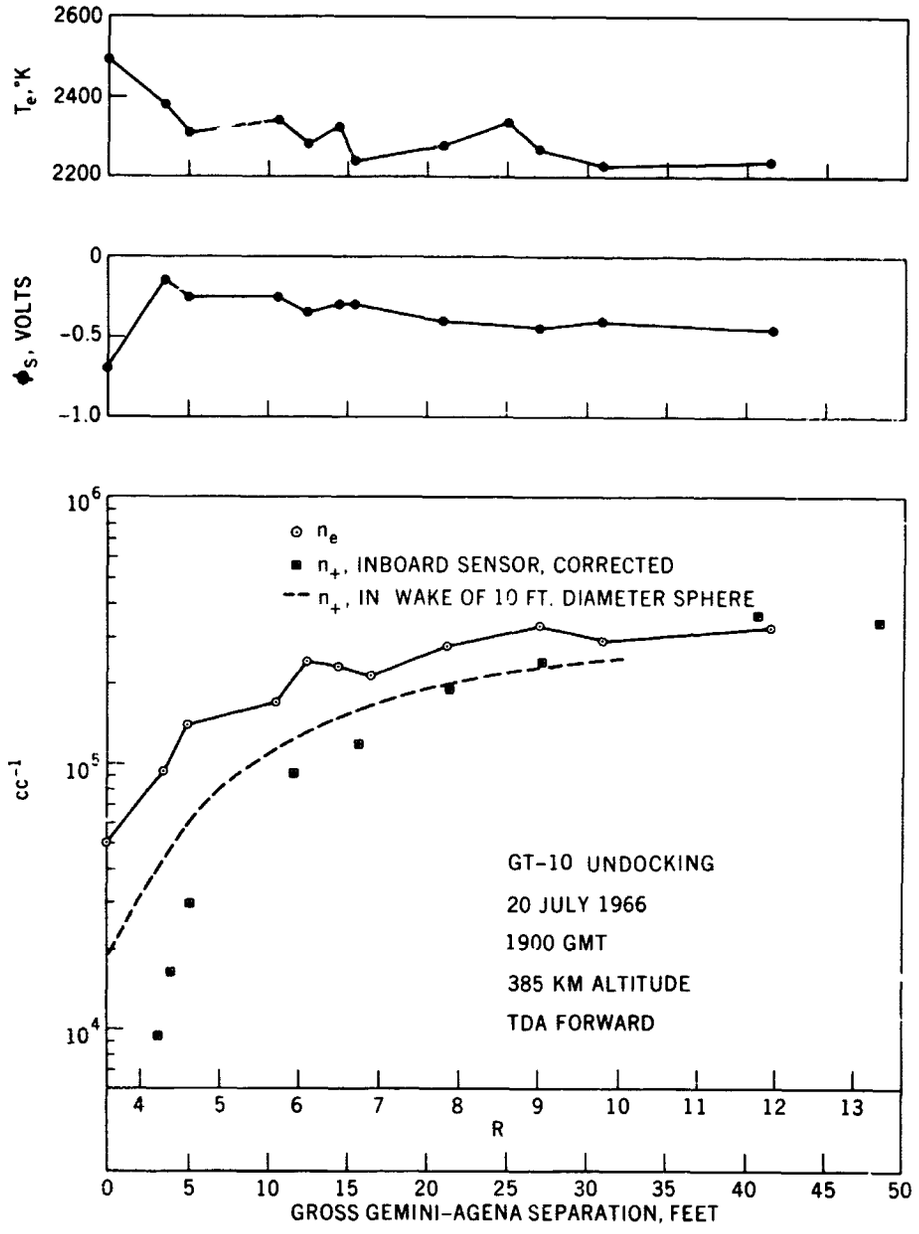

Figure 19. Axial Wake Profile for ϕ_s, T_e, and Densities

CONCLUSIONS

The following conclusions can be drawn from data derived from the Gemini 10 undocking maneuver:

- Undocking occurred when ambient n_e was increasing and ambient T_e was decreasing. Local time was 1530, and the spacecraft had just passed maximum latitude.

- The parameters ϕ_s, T_e, n_e and corrected n_+ (inboard) changed after undocking, reaching stable values after a spacecraft separation of about 30 feet, or about $10 R_0$ behind the forward end of the Gemini. Changes in density and temperatures during undocking were rapid compared to changes in the ambient parameters.

- T_e was higher in the wake than outside the wake.

- The measured densities increased smoothly as the undocking occurred. A comparison between the measured densities and a theoretical density profile in the wake of a sphere yields qualitatively correct results.

THE GEMINI 11 FLIGHT

The S-26 experiment was also performed on Gemini 11 in September 1966. The planned wake maneuvers were successfully carried out and the data were recorded. However, the movie camera, voice tape, and other sources of information for deriving relative position failed or partially failed. No satisfactory time history of relative position has been attained from the small amount of information available. If this problem can be solved, data from Gemini 11 should give a much better picture of the wake than data from Gemini 10 gave.

REFERENCES

1. Al'pert, Ya L., A. V. Gurevich, and L. P. Pitaevsky. Space Physics with Artificial Satellites. Consultants Bureau, New York. 1965

2. Walker, E. H. in Interactions of Space Vehicles with an Ionized Atmosphere. (S. F. Singer, ed.) Pergamon Press, 1965

3. Whipple, E. C. The Equilibrium Electric Potential of a Body in the Upper Atmosphere and in Interplanetary Space. George Washington University PhD Thesis, 1965

4. Samir, U. Interactions of Spacecraft with the Ionosphere. University College PhD Thesis. London, 1966

5. de Leeaw, J. H. Proceedings of the Fifth International Conference on Rarefied Gas Dynamics. (C. L. Brundin, ed.) II, 1561. Academic Press, 1967

6. Shea, J. J. ibid., 1671

7. Liu, V. C. "Ionospheric Gas Dynamics of Satellites and Diagnostic Probes." To be published in Space Sci. Rev. 1969

8. Cox, R. N. in Proceedings of the Third International Conference on Rarefied Gas Dynamics. (J. Laurmann, ed.) II, 1. Academic Press, 1963

9. Hall, D. F., R. F. Kemp, and J. M. Sellen Jr. "Plasma-vehicle Interaction in a Plasma Stream." AIAA Journal. II, 1032. 1964

10. Shkarofsky, P. "Laboratory Simulation of Disturbances Produced by Bodies Moving through a Plasma and of the Solar Wind - Magnetosphere Interaction." Astronautica Acta. XI, 169. 1965

11. Bourdeau, R. E. "On the Interaction between a Spacecraft and an Ionized Medium." Space Sci. Rev. 1, 719. 1963

12. Bourdeau, R. E. and J. L. Donley. "Explorer VIII Satellite Measurements in the Upper Ionosphere." Proc. Roy. Soc. ACCLXXXI, 285. 1965

13. Samir, U. and A. P. Willmore. "The Distribution of Charged Particles near a Moving Spacecraft." Plan. Space Sci. XIII, 285. 1965

14. Samir, U. and A. P. Willmore. "The Equilibrium Potential of a Spacecraft in the Ionosphere." Plan. Space Sci. XIII, 1131. 1966

15. Henderson, C. L. and U. Samir. "Observations of the Disturbed Region around an Ionospheric Spacecraft." Plan. Space Sci. XV, 1499. 1967

16. Hoffmann, J. H. "Composition Measurements of the Topside Ionosphere." Science. CLV, 322. 1967

17. Brace, L. H. and P. L. Dyson. "Documentation of Explorer 32 Electron Temperature Measurements used in Comparisons with Backscatter Measurements at Jicamarca." NASA X-621-68-469. 1968

18. Samir, U. "Spacecraft Plasma Interactions." Spaceflight. X, 285. 1968

19. Medved, D. B., B. E. Troy, and U. Samir. "In-situ Measurements of Ionospheric Plasma Relevant to Spacecraft-Space Plasma Interactions." In preparation, 1969

20. Oya, H. "Ionospheric Plasma Disturbances Due to a Moving Space Vehicle." To be published in Plan. Space Sci., 1969

21. Samir, U. and G. L. Wrenn. "The Dependence of Charge and Potential Distribution around a Spacecraft on Ionic Composition." To be published in Plan. Space Sci., 1969